A Floating-Gate OTFT-Driven AMOLED Pixel Circuit for Variation and Degradation Compensation in Large-Sized Flexible Displays

Tsung-Ching Huang[1], Koichi Ishida[1], Tsuyoshi Sekitani[2], Makoto Takamiya[1], Takao Someya[2], and Takayasu Sakurai[1]

[1]Institute of Industrial Science, University of Tokyo, Japan
[2]Department of Electrical Engineering, University of Tokyo, Japan

ABSTRACT

For the first time, we demonstrate an AMOLED pixel circuit on an 80-μm thick plastic film that applies floating-gate organic TFTs (FG-OTFTs) to compensate for OTFT driving current variations and OLED efficiency degradations. By programming V_{TH} *of the FG-OTFTs, we can realize less than 5% spatial non-uniformity and 85% power reduction compared with voltage-programming.*

1. INTRODUCTION

AMOLED displays have attracted much attention recently because of their excellent image quality and wide viewing angle [1-2]. Organic TFT (OTFT) is considered as a strong candidate for pixel circuits of large-size flexible displays, because of its mechanical flexibility and compatibility with the low-cost printing process at room temperature [3-4]. OTFT-driven AMOLED displays, therefore, are a promising solution for realizing next-generation large-size, light-weight, and mechanically robust flexible displays. To print a large number of OTFTs on large-area flexible substrates with high-uniformity, however, is very challenging and has become the major bottleneck for realizing large-sized OTFT-driven AMOLED flexible displays.

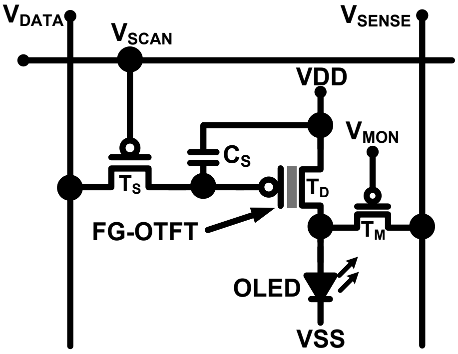

Figure 1: Proposed AMOLED 3T-1C pixel-circuit.

In this paper, for the first time, we demonstrate a FG-OTFT-driven AMOLED pixel circuit for flexible displays as shown in Fig. 1. The pixel circuit enables electrical feedback to tune V_{TH} of the FG-OTFT for compensating OTFT variations and OLED efficiency degradations. Unlike voltage-programming or current-programming [5-6] that require V_{TH} compensation in every frame time, the programmed V_{TH} in our FG-OTFTs can retain for tens of hours and no further V_{TH} programming is needed within the retention time. The proposed work, therefore, has several key advantages over conventional methods including: 1) low power-consumption by eliminating V_{TH} compensation cycle in the frame time, 2) compensation for both OTFT non-uniformity and OLED efficiency degradation, and 3) higher aperture ratio and yield because of reduced transistor counts (3T-1C).

1.1 Floating-Gate Organic TFTs

Fig. 2 shows the cross-section of a 20V FG-OTFT. The channel length L is 20 μm and the organic semiconductor in our p-type FG-OTFT is DNTT [7] with carrier mobility of 0.7 cm^2/Vs. While the 20V FG-OTFT can work as a normal OTFT with -20V gate-voltage V_{GS}, its V_{TH} can be adjusted by applying high-voltage electrical stresses to the gate terminal. As shown in Fig. 3, when the source and drain terminals of a FG-OTFT are grounded and no drain-source current is conducting, the electron holes can be injected from the Parylene gate insulator to the Au floating gate by applying a pulsed high voltage such as -60V to its gate terminal. These injected holes can be kept in the Au floating-gate and reduce electrical field from the gate voltage to the organic semiconductor. The effective V_{TH} of the FG-OTFT is therefore increased until the injected electron holes completely escape. More details about our FG-OTFTs can be found elsewhere in [8].

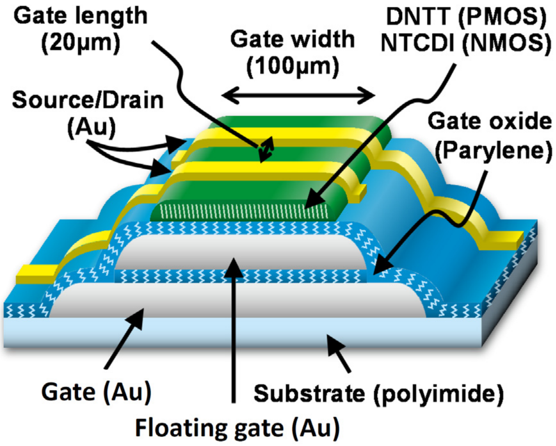

Figure 2: Cross section of a 20V FG-OTFT.

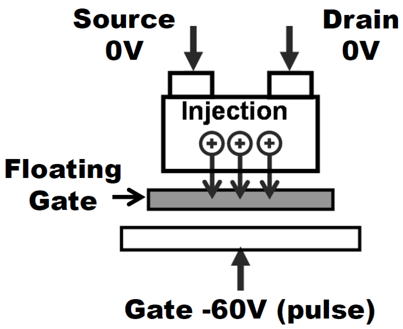

Figure 3: Working principle of a FG-OTFT.

1.2 Pixel Circuit

Fig. 4 shows typical voltages of V_{DATA}, V_{SCAN}, V_{MON}, and V_{SENSE} in Fig. 1 for monitoring FG-OTFT non-uniformity and OLED efficiency degradations, as well as programming V_{TH} of the FG-OTFT. In order to monitor the driving current of T_D as shown in Fig. 4(a) without being affected by V_{TH} variations of T_M, V_{CAL} was set sufficiently close to V_{TH} of T_D while V_G of T_M was set to a higher voltage such as -40V to keep the on-resistance of T_D much higher than that of T_M as shown in Fig. 4(a). SPICE simulations show that the current measurement error can be minimized to less than 5% even under 20% V_{TH} variations of T_M because the measured current was mainly determined by T_D in the saturation region rather than T_M in the linear region. Fig. 4(b) shows the configuration of monitoring OLED efficiency degradation. T_D was switched off by setting V_{GS} of T_D to be 10V and V_{SENSE} was set close to V_{TH} of OLED (~6V) to minimize V_{DS} of T_M for reducing current measurement errors. The OLED efficiency degradation can be estimated by measuring V_{TH} of OLED at a given current. V_{DATA} and V_{TH} of T_D can then be adjusted accordingly to compensate for OLED efficiency degradations.

Fig. 4(c) shows the configuration of V_{TH} programming for T_D. A pulsed electrical stress -60V was applied to the gate terminal of T_D through T_S. V_{DS} of T_D was set to 0V during V_{TH} programming process such that no current is conducting through T_D. The measurement results and the scheme of V_{TH} programming for minimizing non-uniformity and power consumption are followed.

2. MEASUREMENT RESULTS

2.1 V_{TH} Programming

To perform quantitative analysis of V_{TH} programming, we applied a digital control method by fixing the stress voltage V_{STRESS} to -60V and varying the number of stress pulses and the pulse-width for V_{TH} control. Fig. 5 shows the measurement results of the FG-OTFT driving currents during V_{TH} programming process with (-60V, 75ms) stress conditions. The device size of the FG-OTFT was made large to provide sufficient driving currents for our OLEDs to achieve peak brightness greater than 200 cd/m^2. From Fig. 5, we can observe that V_{TH} increases with the stress time due to injected electron holes in the floating-gate. The programmed V_{TH} can retain for tens of hours until full recovery to its original V_{TH}. Since V_{DS} of the T_D was kept to 0V during V_{TH} programming, the measured drain-source current I_{DS} of T_D during V_{TH} programming was lower than 1nA, which was six orders or less than its saturation current and therefore consumed negligible power compared with voltage programming scheme.

Fig. 6 shows the relationship among $\Delta V_{TH,}$ stress pulse width, and stress time with -60V stress voltage. Here V_{TH} is defined as (W/L x 50nA) using the constant

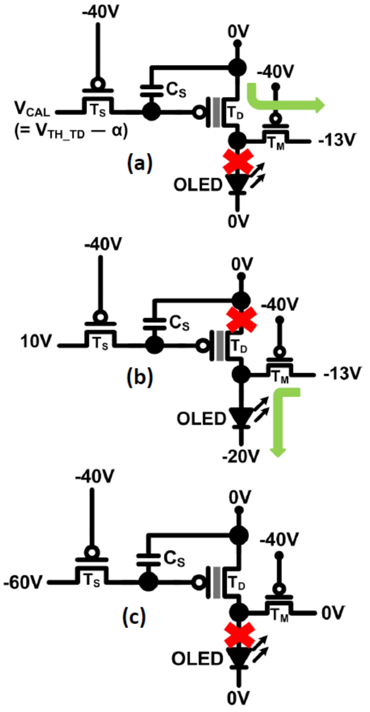

Figure 4: (a) Monitoring FG-OTFT driving current, (b) monitoring OLED efficiency degradations, and (c) applying electrical stress for V_{TH} programming. W_{TD} = 6 cm, W_{TM}=W_{TS}=0.3 cm, and C_S=2pF in our pixels.

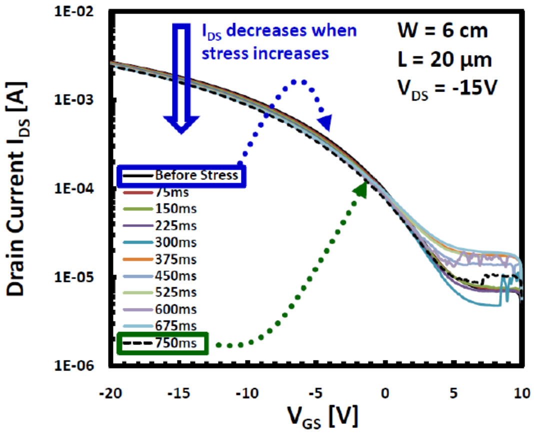

Figure 5: V_{TH} programming process for a FG-OTFT with (-60V, 75ms) step size of electrical stress.

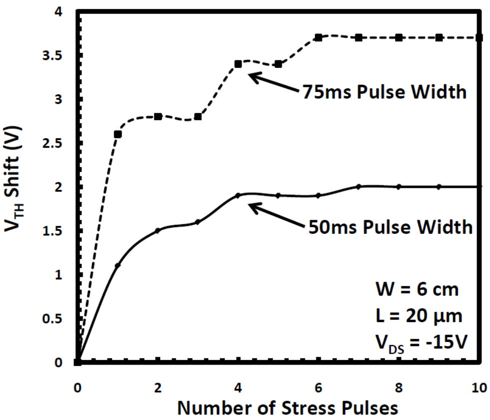

Figure 6: The relationship between V_{TH} shifts and pulse width

current method, where W is the channel width and L is the channel length. We can learn from Fig. 6 that larger stress voltage V_{STRESS} and longer stress time T_{STRESS} can result in greater V_{TH} shifts. The measured ΔV_{TH} can be fitted to Eqn.1 where α and β are fitting parameters.

$$\Delta V_{TH} = {V_{Stress}}^{\alpha} \log_{\beta}(T_{Stress}) \qquad (1)$$

2.2 Variation Compensation for Pixel Circuit

To demonstrate variation compensation by V_{TH} programming, we prepared six identical FG-OTFT-driven AMOLED pixels in a 2x3 array on the same polyimide plastic film. The V_{TH} programming scheme for variations and degradations compensation is illustrated using a flowchart as shown in Fig. 7. V_{TH} monitoring and electrical stress are provided through external circuitry. T_D in Fig. 7 represents the FG-OTFT-based OLED driver as shown in Fig. 4. Fig. 8 shows the compensation results for all six AMOLED pixels. The broken lines represent the initial driving currents provided by FG-OTFTs before V_{TH} programming while solid lines are driving currents after V_{TH} programming, which scheme is illustrated in Fig. 7. The inset of Fig. 8 shows that the driving current variation, represented by standard deviations, was reduced from 14% to less than 5% after V_{TH} programming. Although here only shows the results for total six pixels, the V_{TH} programming scheme can be readily applied to the entire active-matrix of AMOLED flexible displays for minimizing spatial non-uniformity.

The OLED efficiency degradations can also be compensated by monitoring V_{TH} of OLEDs at known input currents through T_M as shown in Fig. 4(b), which can be used to indicate the degree of OLED efficiency degradations for T_D current compensations.

2.3 Power Reduction

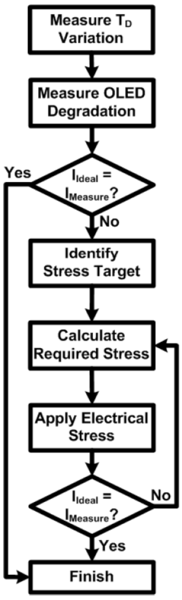

Figure 7: Flowchart of measuring and compensating OTFT variations and OLED degradations.

In addition to variation and degradation compensation, the proposed FG-OTFT pixel circuit also lowers the pixel power consumption P_{PIXEL} because of eliminating the V_{TH} compensation cycle in the frame time τ_{FRAME} (τ_F). For conventional compensation schemes such as voltage programming, V_{TH} of the driving TFT is generated and stored in a capacitor that needs to be updated every frame time. In order to ensure that the stored V_{TH} is equal or close enough to the real V_{TH}, the required compensation time $\tau_{COMPENSATION}$ (τ_C) should be longer than tens of micro-second (µs) [9]. Since τ_C reduces the driving time $\tau_{DRIVING}$ (τ_D) as illustrated in Eqn. 2 for a given τ_F and the compensation power $P_{COMPENSATION}$ (P_C) does not directly contribute to driving the OLED, the required P_{PIXEL} for the voltage-programming scheme within the

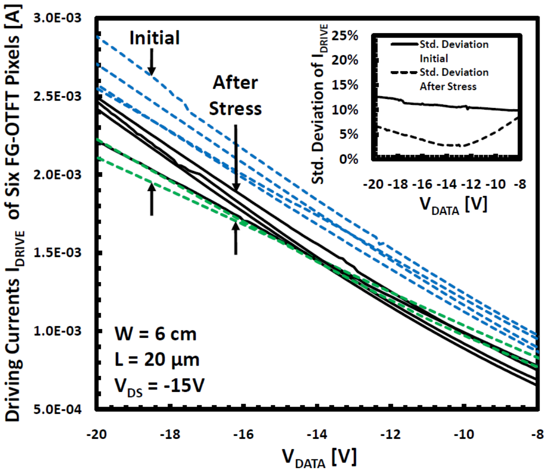

Figure 8: Driving currents I_{DRIVE} of total six pixels before-stress (broken-line) and after-stress (solid-line). The inset shows the standard deviations of I_{DRIVE}. Green broken lines show no-need-to-stress pixels due to initially lower driving currents.

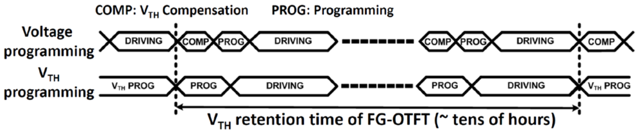

Figure 9: Timing diagram for conventional voltage-programming and proposed V_{TH} programming schemes. V_{TH} programming process can retain V_{TH} for tens of hours.

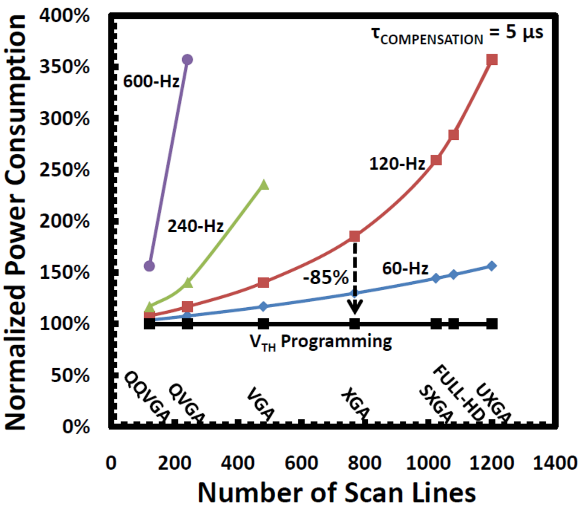

Figure 10: Normalized power consumption P_{PIXEL} of an AMOLED pixel under different display resolutions and refresh rates using voltage-programming scheme. Proposed V_{TH} programming is used as the reference for comparisons.

reduced τ_D in order to achieve the same peak brightness as the proposed V_{TH} programming scheme will therefore increase significantly. Fig. 9 shows the timing diagram and Fig. 10 shows the normalized pixel power consumption P_{PIXEL} for both voltage-programming and V_{TH} programming schemes. Note that P_{PIXEL} in Fig. 10 is calculated by assuming τ_C equal to 5 μs and the same pixel energy consumption E_{PIXEL} under the same τ_F for both cases. While the proposed V_{TH} programming scheme using FG-OTFTs does not require the V_{TH} compensation cycle and consumes negligible compensation power during the V_{TH} programming process, the voltage-programming scheme requires 85% power overhead if driven at the XGA resolution with 120-Hz refresh rate. Higher resolutions and refresh rates, as well as longer τ_C, will inevitably increase the pixel power consumption due to the reduced τ_D. Note that for very high refresh rates such as 240-Hz and 600-Hz, higher resolutions than VGA mode are unable to achieve in the voltage-programming scheme since τ_F will be less than 5 μs minimum requirements of τ_C .

$$P_{PIXEL} = P_{COMPENSATION} + P_{PROGRAMMING} + P_{DRIVING} \qquad (2)$$

$$\tau_{DRIVING} = \tau_{FRAME} - \tau_{COMPENSATION} - \tau_{PROGRAMMING}$$

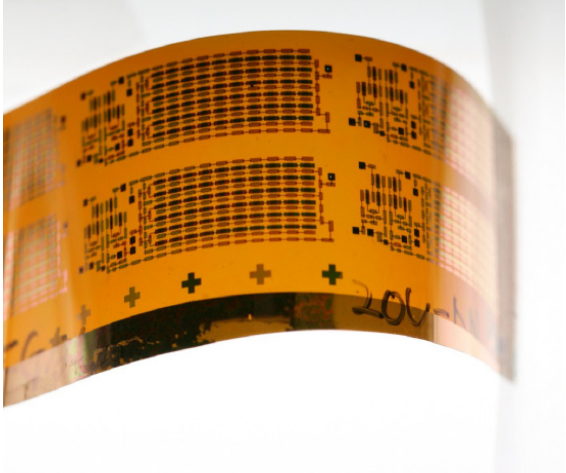

Figure 11: Die photo of the FG-OTFT-driven AMOLED pixels. The pixel size is 20.8 mm x 6.6 mm and substrate thickness is 80-μm.

3. CONCLUSION

In this paper, for the first time, we demonstate a FG-OTFT driven AMOLED pixel circuit on a 80-μm thick polyimide plastic film for compensating OTFT process variations and OLED efficiency degradations. The die photo of the proposed FG-OTFT pixel-circuit is shown in Fig. 11. In our test sample, we prepared six identical pixels allocated as a 2x3 array. After applying the electrical stress to the driving FG-OTFTs, the overall spacial non-uniformity of the driving FG-OTFTs was minimized from 14% to be less than 5%. Compared with the conventional voltage-programming compensation scheme, the pixel power consumption can be reduced by 85% for the XGA resolution at 120-Hz referesh rate.

ACKNOWLEDGEMENT

We will like to thank for Japan Science and Technology Agency (JST) / Core Research for Evolutional Science and Technology (CREST) for financial supports.

REFERENCES

[1] D.-U. Jin et al, SID'09 DIGEST, pp. 983 (2009)
[2] S. Okutani et al, SID'07 DIGEST, pp. 173 (2007)
[3] M. Katsuhara et al, SID'09 DIGEST, pp. 656 (2009)
[4] K. Nomoto, SID'10 DIGEST, pp. 1155 (2010)
[5] A. Nathan et al, IEEE JDT'05, vol.1, iss. 2, pp. 267 (2005)
[6] R. Stewart, SID'10 DIGEST, pp. 790 (2010)
[7] dinaphtho[2,3-b:2',3'-f] thieno [3,2-b] thiophene (DNTT) T. Yamamoto, K. Takimiya, J. Am. Chem. Soc. 2007, 129, 2224.
[8] T. Sekitani et al, Science 326, pp.1516 (2009)
[9] G.R. Chaji et al, IEEE JDT'08, vol.4, iss. 2, pp. 233 (2008)